

Understanding Adam Requires Better Rotation Dependent Assumptions

Lucas Maes^{1,2,†}
Ioannis Mitliagkas^{1,2,5}

Tianyue H. Zhang^{1,2,†}
Damien Scieur^{2,3}

Alexia Jolicoeur-Martineau³
Simon Lacoste-Julien^{1,2,3,4}

Charles Guille-Escuret^{1,2}

¹Mila, Quebec AI Institute

²Université de Montréal

³Samsung SAIL Montreal

⁴Canada CIFAR AI Chair

⁵Archimedes Unit, Athena Research Center

Abstract

Despite its widespread adoption, Adam’s advantage over Stochastic Gradient Descent (SGD) lacks a comprehensive theoretical explanation. This paper investigates Adam’s sensitivity to rotations of the parameter space. We demonstrate that Adam’s performance in training transformers degrades under random rotations of the parameter space, indicating a crucial sensitivity to the choice of basis. This reveals that conventional rotation-invariant assumptions are insufficient to capture Adam’s advantages theoretically. To better understand the rotation-dependent properties that benefit Adam, we also identify structured rotations that preserve or even enhance its empirical performance. We then examine the rotation-dependent assumptions in the literature, evaluating their adequacy in explaining Adam’s behavior across various rotation types. This work highlights the need for new, rotation-dependent theoretical frameworks to fully understand Adam’s empirical success in modern machine learning tasks.

2020; Kaplan et al., 2020). However, this unprecedented growth in model scale has led to a proportional increase in the economic (Dong and Xie, 2024; Sharir et al., 2020; Varoquaux et al., 2024) and environmental (Luccioni et al., 2023, 2019) costs associated with their training.

Despite this clear motivation, Adaptive Moment Estimation (Adam) (Kingma and Ba, 2015) has persisted as the go-to optimizer for language models, with only minor modifications such as AdamW (Loshchilov and Hutter, 2019) becoming widely adopted since Adam’s inception. This success has prompted extensive research to provide theoretical justification for Adam’s performance. While the original convergence proof for Adam was later found to be flawed (Rubio, 2017), recent studies have proposed rigorous convergence proofs under plausible assumptions (Li et al., 2023b; Chen et al., 2019; Défossez et al., 2022).

However, these proofs do not elucidate Adam’s advantages over SGD when training transformer models (Vaswani et al., 2017). Numerous works attempted to explain Adam’s superiority, employing diverse assumptions and analytical frameworks (Zhou et al., 2024; Pan and Li, 2022; Zhang et al., 2024a; Kunstner et al., 2024). The heterogeneity of these approaches has led to a lack of consensus on which theoretical explanations most accurately capture the fundamental mechanisms underlying Adam’s improved performance. For instance, Zhang et al. (2020) suggests it stems from enhanced robustness to heavy-tailed noise, while Kunstner et al. (2023) argues it plays no role.

This study focuses on a fundamental distinction between Adam and SGD: Adam’s dependency on the coordinate system. SGD is rotation-equivariant, i.e., if the loss landscape is rotated, the resulting optimization trajectories from SGD will be the same up to that rotation.

1 INTRODUCTION

Large Language Models (LLMs) have demonstrated remarkable capabilities as their scale grows (Brown et al.,

[†]Equal contributions in alphabetical order

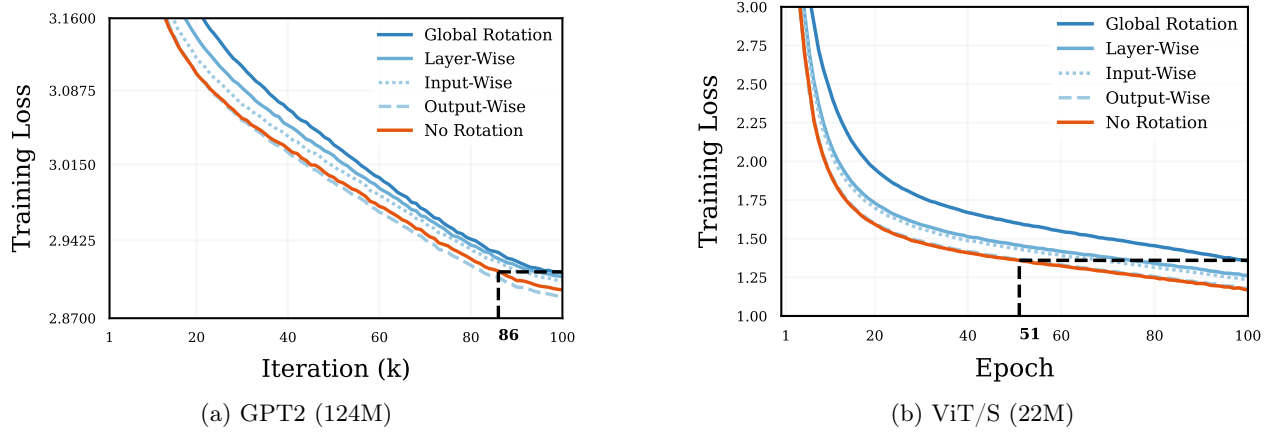


Figure 1: Adam’s performance degrades under certain random rotations of the parameter space, demonstrating its dependence on the standard basis. (a) For GPT2, global rotations lead to a 16% slowdown in training. (b) ViT experiences a more dramatic 96% slowdown under global rotations. Performance is preserved under output-wise rotations but progressively worsens with input-wise, layer-wise, and global rotations, revealing Adam’s increasing sensitivity to coordinate changes of broader scopes. Experimental details are provided in Section 3.1.

In contrast, Adam produces substantially different trajectories. Our experimental investigation reveals that Adam’s performance when training transformers empirically degrades when the objective function undergoes random rotations (Figure 1). This result challenges the adequacy of many existing theoretical frameworks used to analyze Adam’s performance. Indeed, Appendix E shows that most assumptions employed in the literature are rotation-invariant, hence they cannot fully capture or justify Adam’s empirical advantages.

To deepen our understanding of the relationship between basis orientation and Adam’s performance, we address two fundamental questions:

Q1. How do various types of rotations influence Adam’s performance?

We investigate **Q1** by conducting experiments in Section 3, examining Adam’s convergence when rotating specific regions of the parameter space. We also identify some rotations that preserve or enhance Adam’s performance. These findings provide a more nuanced picture of Adam’s adaptive behavior and which properties of the basis are most consequential. Finally, a few rotation-dependent assumptions do exist in the literature. This naturally raises the question:

Q2. Do existing rotation-dependent assumptions adequately captures Adam’s behavior under rotations?

Section 4 examines three assumptions in this context:

L_∞ bounded gradients, Hessian block-diagonality, and L_∞ -smoothness (Xie et al., 2024). Our analysis reveals that while none of these conditions fully capture Adam’s behavior under rotations, L_∞ -smoothness demonstrates some promising characteristics. This highlights the need for more refined theoretical frameworks to model Adam’s performance. These findings pave the way for future research to develop more nuanced, rotation-aware assumptions that better align with Adam’s empirical behavior.

We summarize our **key contributions**:

- **Comprehensive analysis of Adam’s rotation sensitivity:** we conduct in Section 3.1 an empirical study demonstrating Adam’s sensitivity to parameter space rotations, and find a clear correlation between rotation scope (e.g., global, layer-wise) and performance degradation.
- **Identification of performance-enhancing rotations:** we construct in Section 3.2 structured rotations capable of enhancing the convergence of Adam, with potential for future algorithmic contributions.
- **Challenging rotation dependent assumptions:** we assess the applicability of rotation dependent properties in the literature by examining them jointly with our experimental study, and find that existing theoretical frameworks are not properly equipped to fully understand the beneficial properties of Adam.

2 PRELIMINARIES

2.1 Notations and Settings

Let $f : \mathbb{R}^d \rightarrow \mathbb{R}$ be the loss of a neural network with d trainable parameters. Stochastic optimization algorithms approximate $\arg \min_{w \in \mathbb{R}^d} f(w)$ by only accessing independent stochastic functions f_B that depend on a stochastic minibatch B following some data distribution \mathcal{D} such that $\forall w \in \mathbb{R}^d, \mathbb{E}_{B \sim \mathcal{D}}[f_B(w)] = f(w)$.

Our study examines the optimization process under **rotations of the parameter space**. More formally, let $SO(d)$ be the set of rotation matrices,

$$SO(d) = \{\mathbf{R} \in \mathbb{R}^{d \times d} : \mathbf{R}^\top \mathbf{R} = \mathbf{R} \mathbf{R}^\top = \mathbf{I}, \det(\mathbf{R}) = 1\}. \quad (1)$$

Instead of directly optimizing f , we consider its rotated counterpart $f^{(\mathbf{R})} : w \rightarrow f(\mathbf{R}^\top w)$, $\mathbf{R} \in SO(d)$. This transformation rotates the coordinate system while preserving the geometry of the optimization landscape.

Unless specified otherwise, we use the popular AdamW variant of Adam (see Appendix D).

2.2 Rotational Equivariance of SGD

We say that an optimizer is **rotation equivariant** if, after a rotation of the parameter space, its trajectories are equally rotated.

Definition 1 (Rotational equivariance). *Consider an optimization algorithm \mathcal{A} applied to the function f , generating iterates as follow:*

$$w_{t+1} = \mathcal{A}(\{w_i\}_{i=0 \dots t}, f, t).$$

*we say that the optimization algorithm is **rotation equivariant** if it satisfies, $\forall \mathbf{R} \in SO(d)$,*

$$\mathbf{R} w_{t+1} = \mathcal{A}(\{\mathbf{R} w_i\}_{i=0 \dots t}, f^{(\mathbf{R})}, t).$$

Proposition 1. *Stochastic Gradient Descent is rotation-equivariant.*

Proof. Using the same notation as in Section 2.1, we consider SGD* with learning rate η and a fixed sequence of batches B_t :

$$z_{t+1} = \mathcal{A}(z_t, f, t) = z_t - \eta \nabla f_{B_t}(z_t),$$

For any $w_0 \in \mathbb{R}^d$, we have $\mathbf{R} w_0 = \mathcal{A}(\mathbf{R} w_0, f^{(\mathbf{R})}, 0)$. Moreover, we have $\nabla f_{B_t}^{(\mathbf{R})}(w_t) = \mathbf{R} \nabla f_{B_t}(\mathbf{R}^\top w_t)$, hence

$$\begin{aligned} \mathcal{A}(\mathbf{R} z_t, f^{(\mathbf{R})}, t) &= \mathbf{R} z_t - \eta \mathbf{R} \nabla f_{B_t}(\mathbf{R}^\top \mathbf{R} z_t) \\ &= \mathbf{R} z_t - \eta \mathbf{R} \nabla f_{B_t}(z_t) \\ &= \mathbf{R} \mathcal{A}(z_t, f, t) = \mathbf{R} z_{t+1}. \end{aligned}$$

*For the sake of simplicity we are not considering momentum here, but the results similarly hold for heavy ball (Polyak, 1964) and Nesterov Accelerated Gradient (Nesterov, 1983).

matching Definition 1. □

In contrast, as illustrated in Figure 2, Adam is not rotation equivariant. This dependence stems from its element-wise division, see Algorithm 2, step 9 in Appendix D.

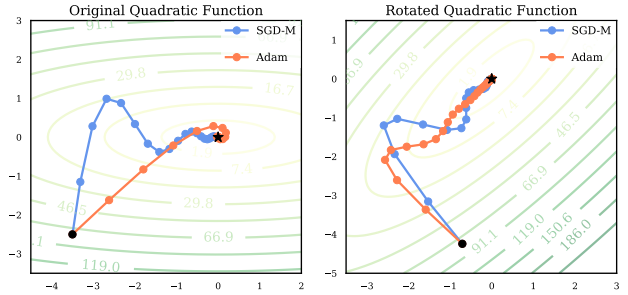


Figure 2: (left) Trajectories of SGD-momentum and Adam on a quadratic function with eigenvectors aligned with coordinates. (right) Trajectories on the same function after rotation. Unlike Adam, SGD-momentum exhibits rotation equivariance, maintaining its trajectory relative to the objective function in both scenarios.

2.3 Training Neural Networks in Rotated Parameter Spaces

A crucial aspect of our study is the empirical evaluation of Adam’s performance under rotations of the parameter space.

Our approach, described in Figure 3, maintains the weights w_t in the standard basis while performing Adam’s optimization steps in the rotated space. This method allows us to leverage existing neural network frameworks for forward and backward propagation while still examining Adam’s behavior under rotation.

Rotations in high dimension. It is computationally intractable to operate with full $d \times d$ rotation matrices due to the size of modern neural networks.

We employ a composite approach that combines block-diagonal rotations with strategic permutations to circumvent this limitation while preserving the essential characteristics of uniformly sampled rotations. This method effectively emulates the statistical properties of full-scale rotations. A detailed description of our sampling process and ablation studies are provided in Appendix A.

Numerical considerations. Given the sensitivity of neural network training to numerical precision (Li et al., 2018; Wang et al., 2018; Sun et al., 2022), it is crucial to ensure that rounding errors from applying

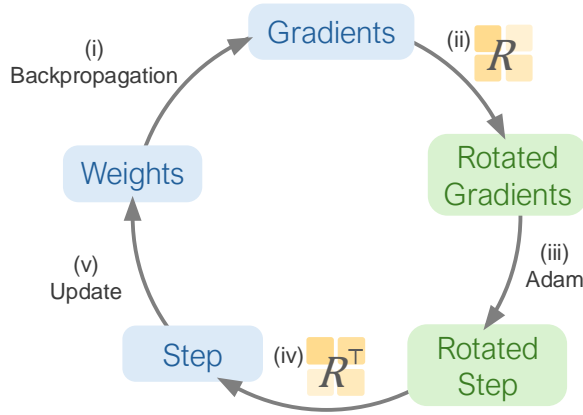


Figure 3: Methodology to train neural networks under rotations of the parameter space. (i) Forward and backward passes in the standard space to retrieve the gradients. (ii) The gradients are rotated using the rotation \mathbf{R} . (iii) Adam receives the rotated gradients and produces an update $\Delta w^{(\mathbf{R})}$ in the rotated space. (iv) $\Delta w^{(\mathbf{R})}$ is rotated back to the original space using \mathbf{R}^\top . (v) The parameters are updated with $\mathbf{R}^\top \Delta w^{(\mathbf{R})}$.

rotations to the gradient do not significantly confound the impact of the change of basis. In particular:

- We apply rotations in single precision.
- We refrain from using FlashAttention (Dao et al., 2022), which was found to increase numeric deviations (Golden et al., 2024).

We validate our methodology with several ablations in Appendix A.

3 ROTATIONS’ INFLUENCE ON ADAM’S EFFICIENCY

This examines the effects of random rotations at different scopes, from neuron-wise to global rotations (Section 3.1) and reveals that specific, structured rotations enhance Adam’s performance (Section 3.2).

3.1 Random Rotations

This section examines the impact of four random rotations in the parameter space on Adam’s performance.

Global Rotation: Applies the rotation to the entire parameter space.

Layer-wise Rotation: We partition the parameter space by layers (for transformers, the keys, queries, and values are considered separate layers), independently rotating each corresponding subspace.

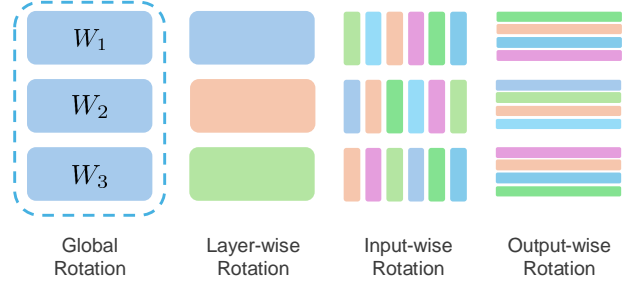


Figure 4: Illustration of different rotation scopes for a model with weights $\mathcal{W} \triangleq \{\mathbf{W}_1, \mathbf{W}_2, \mathbf{W}_3\}$. Global rotation rotates the entire parameter space at once, layer-wise only performs rotations within each layer subspace, and input-wise (resp. output-wise) rotates within the weights originating from a same input neuron (resp. leading to a same output neuron).

Output-wise: Similar to layer-wise, except we partition the parameter space by output neuron. We apply rotations to the weight dimensions corresponding to connections terminating at the same neuron in the subsequent layer.

Input-wise: Same as output-wise, except we rotate weight dimensions *originating* from a same neuron.

Experimental setting. Our approach to sampling high-dimensional rotations is detailed in Appendix A, and Figure 4 illustrates the different scopes of rotations. We conduct experiments across three distinct settings, and technical details such as hyperparameters are provided in Appendix B.

1. **Language Model (GPT-2, Fig. 1a):** We use a 124M-parameters decoder-only transformer (Radford et al., 2019) model on the OpenWebText dataset (Gokaslan and Cohen, 2019), a canonical setup for evaluating large language models.
2. **Image Classification (Transformer, Fig. 1b):** We use a small Vision Transformer (ViT/S, 22M parameters) (Dosovitskiy et al., 2021) for image classification on ImageNet-1K (Deng et al., 2009), exemplifying modern, attention-based computer vision architectures.
3. **Image Classification (ResNet, Fig. B):** We employ a ResNet-50 (He et al., 2016) for image classification on ImageNet-1K, a setting in which SGD is more competitive than Adam (Keskar and Socher, 2017; Wilson et al., 2017).

Results. We make several key observations.

1. Adam’s performance degrades under global rota-

tions across all settings, confirming that the standard basis possesses advantageous properties.

2. The performance further degrades with broader rotation scopes. Layer-wise rotations, which preserve some basis structure, consistently outperform global rotations, highlighting the importance of local coordinate alignment.
3. ResNet exhibits minimal performance degradation under rotations. This reduced sensitivity suggests Adam obtains limited benefit from the standard basis structure in ResNets, explaining its historically inferior performance in training these networks.
4. Output-wise rotations show no significant degradation across all settings, with GPT2 even slightly improving. This suggests that Adam’s adaptivity within output neurons is minimal, supporting recent approaches to reduce redundancy in Adam’s second moments (Zhang et al., 2024b).

Seminal works (Zhang et al., 2024a,b) have highlighted the heterogeneity across different parameter block types in Transformer architectures. In Appendix C, we restrict rotations to specific parameter types and study their individual impact on Adam’s rotation sensitivity.

Given the performance preservation under output-wise rotations, we hypothesize that other specific rotations would preserve or even enhance Adam’s convergence.

3.2 SVD Rotations Improve Performances

Inspired by GaLore (Zhao et al., 2024), which uses low-rank Singular Value Decomposition (SVD) to compress optimizer states, we extend this concept to full-rank SVD to rotate the parameter space. Our approach decomposes the gradient matrix \mathbf{G} of each layer into $\mathbf{G} = \mathbf{U}\mathbf{S}\mathbf{V}^\top$. This decomposition yields a natural rotation of the parameter space through the transformation $\mathbf{M} \rightarrow \mathbf{U}^\top \mathbf{M} \mathbf{V}$, which combines an output-wise rotation (via \mathbf{U}^\top) and an input-wise rotation (via \mathbf{V}). To evaluate this method, we train a GPT2 model under the same conditions as in Section 3.1, but in this SVD-rotated space. We update the SVD decompositions every 200 steps.

Our experiments (see Fig. 5) demonstrate that Adam’s performance improves under SVD rotations. Given its relatively small computational overhead, future research could show that variations of this approach can lead to consistent, cost-effective improvements across different settings.

Our findings underscore the importance of capturing the properties of the chosen basis to understand Adam’s

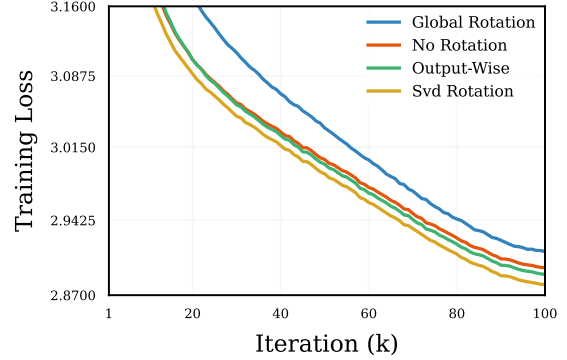


Figure 5: Performance of GPT2 trained with Adam in SVD-rotated space, without rotations, with random output-wise rotation and with random global rotation. The rotations computed with SVD lead to sizeable improvement over the standard basis.

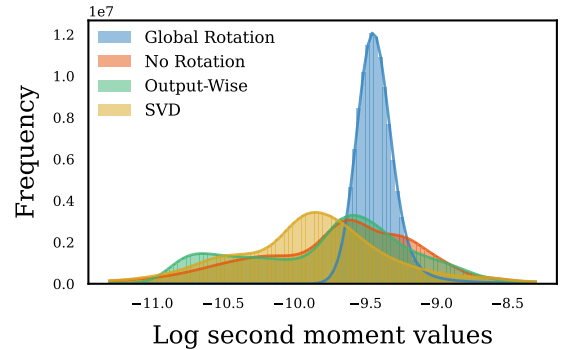


Figure 6: Distribution of second moment values for the final checkpoint of a GPT2 model trained with Adam in various rotated spaces.

performance theoretically. To this end, Figure 6 illustrates the distribution of second moments after training under various rotations. Under random global rotations, Adam’s second moments exhibit a more concentrated distribution. This concentration implies less variation in effective learning rates across dimensions, indicating reduced adaptivity. This reduced adaptivity directly explains the performance degradation observed under global rotations. However, the benefits of SVD rotations are not immediately apparent from the second moment values alone, suggesting a more complex relationship between the parameter space and Adam’s adaptive behavior.

4 EXAMINING ROTATION DEPENDENT ASSUMPTIONS

While rotation-invariant assumptions dominate optimization literature, some frameworks incorporate

rotation-dependent properties. This section examines whether these existing assumptions adequately capture Adam’s rotation dependency: **(i)** it must be realistic in practical settings, and **(ii)** it should align with Adam’s performance. Specifically, the assumption should hold (or have favorable constants) under rotations that improve performance and break down (or have unfavorable constants) under rotations that hinder performance.

We focus on three prominent assumptions: L_∞ bounded gradients (Sec. 4.1), Block-diagonality of the Hessian (Sec. 4.2), and L_∞ -smoothness (Sec. 4.3). We determine whether those assumptions meet criteria **(i)** and **(ii)** and, consequently, their utility in explaining Adam’s behavior under various coordinate transformations. All results presented in this section are derived from experiments training GPT2 on the OpenWebText dataset, as detailed in Section 3.1.

4.1 L_∞ bounded gradients

Reddi et al. (2018); Kingma and Ba (2015) assume a bound on the L_∞ norm of stochastic gradients,

$$\forall w \in \mathbb{R}^d, \|\nabla f_B(w)\|_\infty \leq C \quad \text{almost surely.} \quad (2)$$

The constant C depends on the basis as the L_∞ norm is not preserved under rotations. To evaluate this assumption’s relevance to Adam’s performance, we compute the empirical bound on the rotated gradients:

$$\tilde{C}_{\mathbf{R}'}(\mathbf{R}) := \max_{B_i} \|\nabla f_{B_i}^{(\mathbf{R})}(w_{\mathbf{R}'})\|_\infty,$$

where $w_{\mathbf{R}'}$ denotes the last checkpoint obtained by running Adam under rotation \mathbf{R}' . The maximum is over 1000 stochastic minibatches B_i , across different rotations \mathbf{R} (see Section 3). Table 1 reveals that \tilde{C} significantly decreases under random global rotations, predicting better performance for Adam, but we observe degradation in Adam’s convergence. This discrepancy shows that the L_∞ gradient bound fails to capture the beneficial properties of the basis for Adam.

\mathbf{R}	None	Global	Output-wise	SVD
\tilde{C}_{None}	0.883	0.015	0.105	0.635
\tilde{C}_{Global}	0.220	0.009	0.220	0.220

Table 1: Empirical L_∞ gradient bound \tilde{C} over 1000 stochastic gradients at the last checkpoint.

4.2 Block-diagonality of the Hessian

A common hypothesis for understanding Adam’s behavior is that the Hessian is well-approximated by a block-diagonal matrix (Zhang et al., 2024a). This

property might correlate with Adam’s performance. Indeed, random rotations likely disrupt block-diagonality, hence degrading Adam’s convergence. However, rotations within parameter spaces corresponding to diagonal blocks would preserve this structure, potentially explaining the consistent performance under random output-wise rotations.

To examine this assumption’s validity, we sample rows of the Hessian of $f^{(\mathbf{R})}$ at a checkpoint $w_{\mathbf{R}'}$:

$$\begin{aligned} \mathbf{r}_i(\mathbf{R}, \mathbf{R}') &= \frac{1}{k} \sum_{j=1}^k \nabla^2 f_{B_j}^{(\mathbf{R})}(w_{\mathbf{R}'})_{[i,:]} \\ &= \frac{1}{k} \sum_{j=1}^k \mathbf{R} \nabla^2 f_{B_j}(w_{\mathbf{R}'}) \cdot \mathbf{R}^\top \mathbf{e}_i, \end{aligned}$$

where \mathbf{e}_i denotes the i^{th} canonical basis vector. The vector \mathbf{r}_i represents the average of the i -th row of the stochastic Hessian over k minibatches. As k increases, \mathbf{r}_i converges to the true Hessian row. We set $k = 5000$ in the experiments. We use efficient Hessian-vector products (hvp) (Dagr  ou et al., 2024) for this computation.

We partition the indices of the Hessian row \mathbf{r}_i corresponding to weight w_i into three disjoint subsets:

$$\mathbf{r}_i = \mathbf{r}_{i[I_N]} + \mathbf{r}_{i[I_L]} + \mathbf{r}_{i[I_{\neq}]}, \quad \text{where}$$

- I_N are indices of weights leading to the same output neuron as w_i ,
- I_L are indices of other weights from the same layer,
- I_{\neq} are indices of weights of other layers,

and $\mathbf{r}_{i[I_N]} = r_i$ (resp. I_L and I_{\neq}) in the indices in I_N (resp. I_L and I_{\neq}) and zero elsewhere.

Figure 7 presents the distribution of absolute values for each subset. Our findings show that entries in I_N and, to a lesser extent, I_L , are significantly larger than those from I_{\neq} , supporting the notion of an approximately block-diagonal Hessian.

To assess the practical implications of this structure, we evaluate how each block contributes to gradient variations for a given small direction δw . This local variation can be approximated and decomposed as:

$$\begin{aligned} [\nabla f(w + \delta w) - \nabla f(w)]_i &\approx \mathbf{e}_i^T \nabla^2 f(w) \delta w \\ &= \mathbf{r}_{i[I_N]} \cdot \delta w + \mathbf{r}_{i[I_L]} \cdot \delta w + \mathbf{r}_{i[I_{\neq}]} \cdot \delta w. \end{aligned}$$

Table 2 quantifies these contributions in either a random direction or Adam’s update direction. Surprisingly, our results reveal that Hessian values outside the block diagonal are the primary drivers of gradient evolution, despite their smaller magnitude.

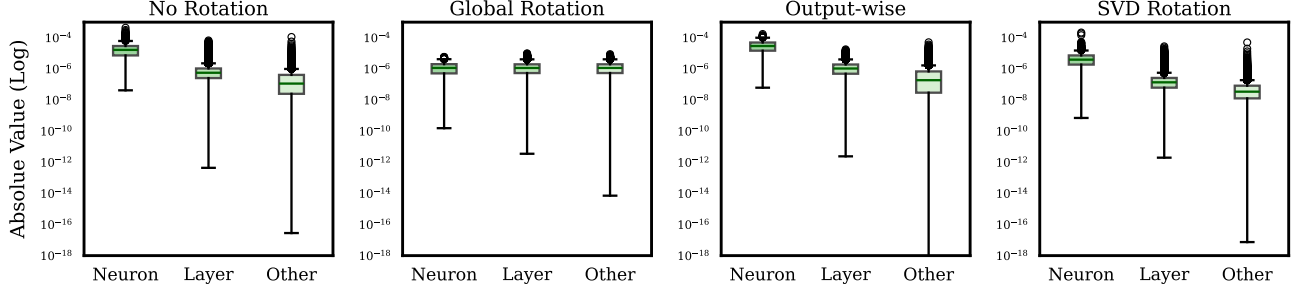


Figure 7: Distribution of Hessian values within output neuron, layer and non-layer in second Transformer block attention projection layer. In no rotation, values within neuron are of magnitude higher than others, presuming a possible block-diagonal structure. The structure is preserved in SVD and output-wise rotations, and lost in global rotation.

δw direction	Random	Update direction
$\mathbf{r}_{i[I_N]} \delta w$ (Neuron)	2.86e-05	-4.60e-10
$\mathbf{r}_{i[I_L]} \delta w$ (Layer)	-8.71e-06	1.30e-08
$\mathbf{r}_{i[I_{\neq}]} \delta w$ (Other)	1.48e-04	2.02e-07

Table 2: Contribution $\mathbf{r}_{i[I]} \cdot \delta w_{[I]}$ of hessian values in block I to the variations of the i -th dimension of the gradient in direction δw . Averaged over multiple samples of δw , either in random directions (left column) or in the direction of the update direction (right column).

This finding challenges the strict block-diagonal Hessian assumption in theoretical analyses. While the diagonal blocks contain larger values, their limited size compared to the full parameter space means that off-diagonal elements collectively play a crucial role in shaping the loss landscape’s geometry.

4.3 L_∞ -smoothness and (1,1)-norm

L_∞ -smoothness was recently shown to guarantee the convergence of Adam, and presented as a potential key property of the basis in Xie et al. (2024). We first remind its definition.

Definition 2. A function f is C -smooth wrt. $\|\cdot\|_\infty$ if $\|\nabla f(x) - \nabla f(y)\|_1 \leq C\|x - y\|_\infty \forall x, y \in \mathbb{R}^d$.

Given the challenges in directly estimating the L_∞ -smoothness constant, Xie et al. (2024) proposed using the (1,1)-norm of the Hessian as a surrogate measure. This norm is defined as:

$$\|H\|_{(1,1)} := \sum_{m=1}^M \sum_{n=1}^N |H_{mn}|,$$

Where H_{mn} represents the element at the m -th row and n -th column of the Hessian matrix. Notably, they observed a degradation in their estimate of $\|H\|_{(1,1)}$ under global random rotations.

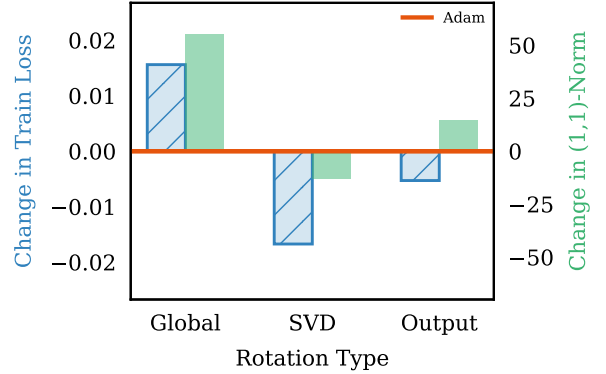


Figure 8: Estimated (1,1)-norm of the Hessian and final accuracy for Global, SVD, and output-wise rotations, presented as differences from the non-rotated baseline. The (1,1) norm seems to correlate with Adam’s performance on global rotations and SVD rotations, but unfortunately degrades on output-wise rotation despite the slight increase in performance.

However, it remains unclear whether this degradation is a universal phenomenon for all rotations of the parameter space or if it specifically correlates with Adam’s performance. To investigate this, we estimate the (1,1)-norm by averaging the L_1 norm of Hessian rows, sampled using the methodology described in Section 4.2.

Figure 8 illustrates the variations in $\|H\|_{(1,1)}$ under global, svd, and output-wise rotations, and yields several significant findings:

- Under global rotations, we confirm the findings of Xie et al. (2024) that the (1,1)-norm also degrades.
- Interestingly, we find that SVD rotations lead to an improvement in the (1,1)-norm. This enhancement correlates positively with the observed boost in Adam’s performance under these rotations, sug-

gesting a potential link between this geometric property and Adam efficiency.

- Unfortunately, a more nuanced picture emerges with output-wise rotations. Despite slight improvements in Adam’s performance, we observe a degradation in the $(1,1)$ -norm.

In light of these results, we conclude that the $(1,1)$ -norm demonstrates promising potential as a metric for understanding Adam’s performance under various coordinate transformations. Its correlation with Adam’s efficiency in certain scenarios, particularly under global and SVD rotations, suggests it captures meaningful aspects of the optimization landscape’s geometry.

However, the discrepancy observed with output-wise rotations indicates that the $(1,1)$ -norm, in its current form, may not fully encapsulate all factors influencing Adam’s behavior. This limitation points to the need for further refinement and possibly the development of complementary metrics.

5 RELATED WORK

Adam under rotations. We consider the concurrent work [Xie et al. \(2024\)](#) to be the closest related study, showing that Adam converges more slowly with a randomly rotated loss landscape. They provide convergence analysis based on L_∞ geometry, demonstrating that this yields a better empirical smoothness constant for GPT-2 models. While their work offers valuable theoretical insights, our study takes a more experimental stance. We aim to paint a comprehensive picture of Adam’s behavior under a spectrum of rotations, from random to structured transformations, and evaluate how existing rotation invariant assumptions correlate with Adam performance.

Understanding Adam. Our work casts light on the critical interactions between Adam and the coordinate system, contributing to a growing body of research on Adam’s behavior and convergence. Recent works have attributed Adam’s success to the heterogeneous block-diagonal structure of its Hessian ([Zhang et al., 2024a](#)), though we find this assumption to be unrealistic. Others have improved convergence guarantees: [Défossez et al. \(2022\)](#) and [Guo et al. \(2022\)](#) offered simplified and novel derivations, [Zhang et al. \(2022\)](#) argued that vanilla Adam converges without modification, [Zhou et al. \(2024\)](#) provided a general convergence analysis for adaptive methods in non-convex settings, and [Li et al. \(2023b\)](#) proposed a convergence proof for Adam without relying on globally bounded gradients. [Li et al. \(2023a\)](#) developed a convergence analysis based on generalized smoothness conditions, and [Hübner et al. \(2023\)](#)

proposed parameter-agnostic convergence results under these relaxed conditions. Finally, lower bounds for non-convex optimization were established by [Arjevani et al. \(2019\)](#), with [Wang et al. \(2023\)](#) addressing the gap between upper and lower bounds for Adam’s iteration complexity.

Adam’s advantages over SGD. Prior works have also attempted to justify Adam’s advantages over SGD. [Zhang et al. \(2020\)](#); [Zhou et al. \(2024\)](#) suggest SGD suffers more from heavy-tailed noise, with Adam converging faster when gradients are sparse. However, [Kunstner et al. \(2023\)](#) found noise reduction through larger batch sizes benefits Adam but not SGD. Additionally, [Kunstner et al. \(2024\)](#) ties Adam’s advantage over SGD in language models to heavy-tailed class imbalance, and [Pan and Li \(2022\)](#) to the concept of directional sharpness.

6 DISCUSSION

6.1 Limitations

While our study demonstrates the critical need for a proper characterization of the beneficial properties of the Hessian in understanding Adam’s performance, it is important to note that we do not propose a specific property that fully captures these benefits. Instead, we lay the groundwork by providing a detailed blueprint for this missing theoretical tool, outlining the key characteristics it should possess, and provide novel insights into the relationship between Adam and the standard base.

6.2 Conclusion

In this work, we have conducted a comprehensive investigation into Adam’s sensitivity to rotations of the parameter space, revealing key insights into its optimization dynamics. We demonstrated that some rotations possess advantageous properties, opening new avenues for algorithmic contributions to adaptive algorithms. Our study demonstrates that Adam’s performance is intricately tied to the choice of basis, a relationship that existing theoretical frameworks struggle to capture adequately. This investigation highlights the limitations of current rotation-invariant assumptions in explaining Adam’s behavior and underscores the need for new, basis-dependent theoretical tools. As the field continues to evolve, we anticipate that these findings will spark new avenues of research, potentially leading to more robust optimization algorithms and deepening our understanding of the fundamental principles underlying successful deep learning optimization.

Acknowledgements

This research was partially supported by the Canada CIFAR AI Chair program (Mila) and Samsung Electronics Co., Ltd. Simon Lacoste-Julien is a CIFAR Associate Fellow in the Learning in Machines & Brains program. We also acknowledge that this research was enabled in part by computing resources, software, and technical assistance provided by Mila and the Digital Research Alliance of Canada. Ioannis Mitliagkas acknowledges support by an NSERC Discovery grant (RGPIN-2019-06512). We would like to thank Adam Ibrahim for his helpful comments and insights, and Ayoub Echchahed, Pedram Khorsandi, Alan Milligan, Ryan d’Orazio and Vitória Barin Pacela for their valuable feedback.

References

- Yossi Arjevani, Yair Carmon, John C. Duchi, Dylan J. Foster, Nathan Srebro, and Blake E. Woodworth. Lower bounds for non-convex stochastic optimization. *Mathematical Programming*, 199:165–214, 2019.
- Lucas Beyer, Xiaohua Zhai, and Alexander Kolesnikov. Better plain vit baselines for imagenet-1k. *arXiv:2205.01580*, 2022.
- Tom Brown, Benjamin Mann, Nick Ryder, Melanie Subbiah, Jared D Kaplan, Prafulla Dhariwal, Arvind Neelakantan, Pranav Shyam, Girish Sastry, Amanda Askell, Sandhini Agarwal, Ariel Herbert-Voss, Gretchen Krueger, Tom Henighan, Rewon Child, Aditya Ramesh, Daniel Ziegler, Jeffrey Wu, Clemens Winter, Chris Hesse, Mark Chen, Eric Sigler, Mateusz Litwin, Scott Gray, Benjamin Chess, Jack Clark, Christopher Berner, Sam McCandlish, Alec Radford, Ilya Sutskever, and Dario Amodei. Language models are few-shot learners. In *Neurips*, 2020.
- Xiangyi Chen, Sijia Liu, Ruoyu Sun, and Mingyi Hong. On the convergence of a class of adam-type algorithms for non-convex optimization. In *ICLR*, 2019.
- Michael Crawshaw, Mingrui Liu, Francesco Orabona, Wei Zhang, and Zhenxun Zhuang. Robustness to unbounded smoothness of generalized signsgd. In *Neurips*, 2022.
- Mathieu Dagr  ou, Pierre Ablin, Samuel Vaiter, and Thomas Moreau. How to compute hessian-vector products? In *ICLR Blogposts*, 2024. URL <https://iclr-blogposts.github.io/2024/blog/bench-hvp/>.
- Tri Dao, Dan Fu, Stefano Ermon, Atri Rudra, and Christopher R  . Flashattention: Fast and memory-efficient exact attention with io-awareness. In *Neurips*, 2022.
- Alexandre D  fossez, Leon Bottou, Francis Bach, and Nicolas Usunier. A simple convergence proof of adam and adagrad. *TMLR*, 2022.
- Jia Deng, Wei Dong, Richard Socher, Li-Jia Li, Kai Li, and Li Fei-Fei. Imagenet: A large-scale hierarchical image database. In *CVPR*, 2009.
- Haiwei Dong and Shuang Xie. Large language models (llms): Deployment, tokenomics and sustainability. *arXiv:2405.17147*, 2024.
- Alexey Dosovitskiy, Lucas Beyer, Alexander Kolesnikov, Dirk Weissenborn, Xiaohua Zhai, Thomas Unterthiner, Mostafa Dehghani, Matthias Minderer, Georg Heigold, Sylvain Gelly, Jakob Uszkoreit, and Neil Houlsby. An image is worth 16x16 words: Transformers for image recognition at scale. In *ICLR*, 2021.
- Aaron Gokaslan and Vanya Cohen. Openweb-text corpus. <http://Skylion007.github.io/OpenWebTextCorpus>, 2019.
- Alicia Golden, Samuel Hsia, Fei Sun, Bilge Acun, Basil Hosmer, Yejin Lee, Zachary DeVito, Jeff Johnson, Gu-Yeon Wei, David Brooks, and Carole-Jean Wu. Is flash attention stable? *arXiv:2405.02803*, 2024.
- Baptiste Goujaud, Adrien Taylor, and Aymeric Dieuleveut. Optimal first-order methods for convex functions with a quadratic upper bound. *arXiv:2205.15033*, 2022.
- Charles Guille-Escuret, Baptiste Goujaud, Manuela Girotti, and Ioannis Mitliagkas. A study of condition numbers for first-order optimization. In *AISTATS*, 2020.
- Charles Guille-Escuret, Adam Ibrahim, Baptiste Goujaud, and Ioannis Mitliagkas. Gradient descent is optimal under lower restricted secant inequality and upper error bound. In *Neurips*, 2022.
- Charles Guille-Escuret, Hiroki Naganuma, Kilian Fatras, and Ioannis Mitliagkas. No wrong turns: The simple geometry of neural networks optimization paths. In *ICML*, 2024.
- Zhishuai Guo, Yi Xu, Wotao Yin, Rong Jin, and Tianbao Yang. A novel convergence analysis for algorithms of the adam family and beyond. *arXiv:2104.14840*, 2022.
- Kaiming He, X. Zhang, Shaoqing Ren, and Jian Sun. Deep residual learning for image recognition. In *CVPR*, 2015.
- Kaiming He, Xiangyu Zhang, Shaoqing Ren, and Jian Sun. Deep residual learning for image recognition. In *CVPR*, 2016.
- Florian H  bler, Junchi YANG, Xiang Li, and Niao He. Parameter-agnostic optimization under relaxed smoothness. In *Neurips workshop OPT: Optimization for Machine Learning*, 2023.

- Jared Kaplan, Sam McCandlish, Tom Henighan, Tom B Brown, Benjamin Chess, Rewon Child, Scott Gray, Alec Radford, Jeffrey Wu, and Dario Amodei. Scaling laws for neural language models. *arXiv:2001.08361*, 2020.
- Andrej Karpathy. NanoGPT, 2022. URL <https://github.com/karpathy/nanoGPT>.
- Nitish Shirish Keskar and Richard Socher. Improving generalization performance by switching from adam to sgd. *arXiv:1712.07628*, 2017.
- Diederik P. Kingma and Jimmy Ba. Adam: A method for stochastic optimization. In *ICLR*, 2015.
- Frederik Kunstner, Jacques Chen, Jonathan Wilder Lavington, and Mark Schmidt. Noise is not the main factor behind the gap between sgd and adam on transformers, but sign descent might be. In *ICLR*, 2023.
- Frederik Kunstner, Robin Yadav, Alan Milligan, Mark Schmidt, and Alberto Bietti. Heavy-tailed class imbalance and why adam outperforms gradient descent on language models. In *Neurips*, 2024.
- Haochuan Li, Jian Qian, Yi Tian, Alexander Rakhlin, and Ali Jadbabaie. Convex and non-convex optimization under generalized smoothness. In *Neurips*, 2023a.
- Haochuan Li, Alexander Rakhlin, and Ali Jadbabaie. Convergence of adam under relaxed assumptions. In *Neurips*, 2023b.
- Huan Li and Zhouchen Lin. On the $o(\frac{\sqrt{d}}{T^{1/4}})$ convergence rate of rmsprop and its momentum extension measured by ℓ_1 norm. *arXiv:2402.00389*, 2024.
- Zhaoqi Li, Yu Ma, Catalina Vajiac, and Yunkai Zhang. Exploration of numerical precision in deep neural networks. *arXiv:1805.01078*, 2018.
- Ilya Loshchilov and Frank Hutter. Decoupled weight decay regularization. In *ICLR*, 2019.
- Alexandra Sasha Luccioni, Sylvain Viguier, and Anne-Laure Ligozat. Estimating the carbon footprint of bloom, a 176b parameter language model. *JMLR*, 24(253):1–15, 2023.
- Sasha Luccioni, Victor Schmidt, Alexandre Lacoste, and Thomas Dandres. Quantifying the carbon emissions of machine learning. In *NeurIPS Workshop on Tackling Climate Change with Machine Learning*, 2019.
- Zhi-Quan Luo and Paul Tseng. Error bounds and convergence analysis of feasible descent methods: a general approach. *Annals of Operations Research*, 46(1):157–178, 1993.
- Francesco Mezzadri. How to generate random matrices from the classical compact groups. *Notices of the American Mathematical Society*, 54:592 – 604, 2007.
- Yurii Nesterov. A method for solving the convex programming problem with convergence rate $o(1/k^2)$. *Proceedings of the USSR Academy of Sciences*, 269: 543–547, 1983.
- Maris Ozols. How to generate a random unitary matrix, 2009. Technical report.
- Yan Pan and Yuanzhi Li. Toward understanding why adam converges faster than SGD for transformers. In *NeurIPS Workshop OPT: Optimization for Machine Learning*, 2022.
- Boris T. Polyak. Gradient methods for the minimisation of functionals. *USSR Computational Mathematics and Mathematical Physics*, 3(4):864 – 878, 1963.
- B.T. Polyak. Some methods of speeding up the convergence of iteration methods. *USSR Computational Mathematics and Mathematical Physics*, 4(5):1–17, 1964.
- Alec Radford, Jeffrey Wu, Rewon Child, David Luan, Dario Amodei, Ilya Sutskever, et al. Language models are unsupervised multitask learners. *OpenAI blog*, 2019.
- Sashank J. Reddi, Satyen Kale, and Sanjiv Kumar. On the convergence of adam and beyond. In *ICLR*, 2018.
- David Martinez Rubio. Convergence analysis of an adaptive method of gradient descent. *University of Oxford, Oxford, M. Sc. thesis*, 2017.
- Or Sharir, Barak Peleg, and Yoav Shoham. The cost of training nlp models: A concise overview. *arXiv:2004.08900*, 2020.
- Yuxin Sun, Dong Lao, Ganesh Sundaramoorthi, and Anthony Yezzi. Surprising instabilities in training deep networks and a theoretical analysis. In *Neurips*, 2022.
- Gaël Varoquaux, Alexandra Sasha Luccioni, and Meredith Whittaker. Hype, sustainability, and the price of the bigger-is-better paradigm in ai. *arXiv:2409.14160*, 2024.
- Ashish Vaswani, Noam Shazeer, Niki Parmar, Jakob Uszkoreit, Llion Jones, Aidan N. Gomez, Łukasz Kaiser, and Illia Polosukhin. Attention is all you need. In *Neurips*, 2017.
- Bohan Wang, Jingwen Fu, Huishuai Zhang, Nanning Zheng, and Wei Chen. Closing the gap between the upper bound and lower bound of adam’s iteration complexity. In *Neurips*, 2023.
- Naigang Wang, Jungwook Choi, Daniel Brand, Chia-Yu Chen, and Kailash Gopalakrishnan. Training deep neural networks with 8-bit floating point numbers. In *Neurips*, 2018.
- Ashia C Wilson, Rebecca Roelofs, Mitchell Stern, Nati Srebro, and Benjamin Recht. The marginal value of

adaptive gradient methods in machine learning. In *Neurips*, 2017.

Shuo Xie, Mohamad Amin Mohamadi, and Zhiyuan Li. Adam exploits ℓ_∞ -geometry of loss landscape via coordinate-wise adaptivity. In *ICML workshop High-dimensional Learning Dynamics: The Emergence of Structure and Reasoning*, 2024.

Jingzhao Zhang, Sai Praneeth Karimireddy, Andreas Veit, Seungyeon Kim, Sashank Reddi, Sanjiv Kumar, and Suvrit Sra. Why are adaptive methods good for attention models? In *Neurips*, 2020.

Yushun Zhang, Congliang Chen, Naichen Shi, Ruoyu Sun, and Zhi-Quan Luo. Adam can converge without any modification on update rules. In *Neurips*, 2022.

Yushun Zhang, Congliang Chen, Tian Ding, Ziniu Li, Ruoyu Sun, and Zhi-Quan Luo. Why transformers need adam: A hessian perspective. In *Neurips*, 2024a.

Yushun Zhang, Congliang Chen, Ziniu Li, Tian Ding, Chenwei Wu, Yinyu Ye, Zhi-Quan Luo, and Ruoyu Sun. Adam-mini: Use fewer learning rates to gain more. *arXiv:2406.16793*, 2024b.

Jiawei Zhao, Zhenyu Zhang, Beidi Chen, Zhangyang Wang, Anima Anandkumar, and Yuandong Tian. Galore: Memory-efficient LLM training by gradient low-rank projection. In *ICLR Workshop on practical ML for limited/low resource settings*, 2024.

Dongruo Zhou, Jinghui Chen, Yuan Cao, Ziyang Yang, and Quanquan Gu. On the convergence of adaptive gradient methods for nonconvex optimization. *TMLR*, 2024.

Fangyu Zou, Li Shen, Zequn Jie, Weizhong Zhang, and Wei Liu. A sufficient condition for convergences of adam and rmsprop. In *CVPR*, 2019.

Appendix

Table of Contents

A SAMPLING RANDOM ROTATIONS IN HIGH DIMENSION	12
A.1 High-Dimensional Rotations	12
A.2 Reflections and Sampling From The Haar Measure	13
A.3 Rotation Residual	13
A.4 Overall Validation and Impact of Flash Attention	14
B EXPERIMENTAL DETAILS	15
B.1 Rotations Design Choices	15
B.2 Architectures	15
B.3 Assumptions Estimation	15
C ADDITIONAL RESULTS	16
C.1 Main Experiments	16
C.2 Architecture Aware Rotation.	17
C.3 Hessian Rows	17
D ADAMW ALGORITHM	21
E COMMON ASSUMPTIONS IN FIRST-ORDER OPTIMIZATION THEORY	21

A SAMPLING RANDOM ROTATIONS IN HIGH DIMENSION

This section explains our method of sampling random rotations for high-dimensional spaces and the implementation details.

A.1 High-Dimensional Rotations

Even small modern machine learning models typically have millions of parameters. Consequently, storing a $d \times d$ rotation matrix is often intractable, let alone performing the dot product required to rotate the gradient vector. To address this issue, we sample a $n \times n$ rotation matrix \mathbf{R}_n with $n \ll d$ uniformly (in the sense of the Haar measure) from the special orthogonal group $SO(n)$, and a random permutation π of $0, \dots, d-1$. For now, we assume $\frac{d}{n} \in \mathbb{N}$, see appendix A.3 for a general case. To rotate a gradient g , we compute:

$$g^{(\mathbf{R}_n, \pi)} := \pi^{-1} \circ \left(\left[\bigoplus_{i=1}^{d/n} R_n \right] (\pi \circ g) \right), \quad (3)$$

$$= \pi^{-1} \circ \begin{bmatrix} R_n & & & \\ & R_n & & 0 \\ & & R_n & \\ 0 & & & \ddots & \\ & & & & R_n \end{bmatrix} (\pi \circ g), \quad (4)$$

where \oplus denotes the direct sum operation, producing a block-diagonal matrix with d/n blocks R_n . This procedure effectively computes a rotation by blocks of size n picked from a random partition of indices, constituting a valid rotation.

Intuitively, if n is sufficiently large, we expect this procedure to approximate well the effect of random rotations sampled uniformly from $SO(d)$, due to the law of large numbers homogenizing geometric properties across coordinates. To confirm this intuition, we perform an ablation study in Figure 9, finding that the impact on Adam’s performance saturates well below our operational values.

Our approximation reduces the memory cost from $O(d^2)$ to $O(n^2 + d)$, and the computational cost from $O(d^2)$ to $O(nd)$. Since batch matrix multiplications required for the rotation can be performed efficiently on modern GPUs, the final overhead of applying rotations is extremely small.

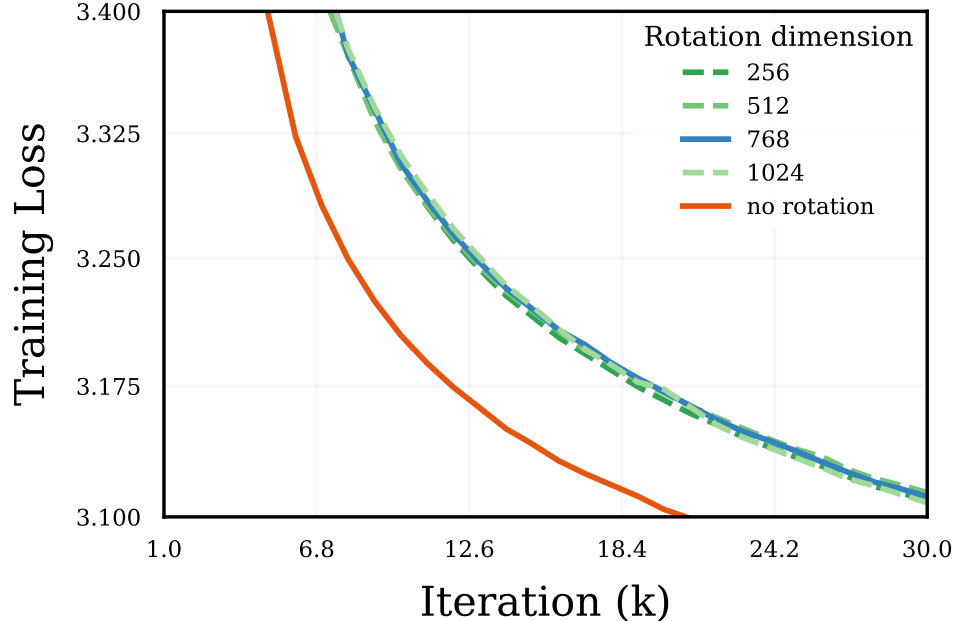


Figure 9: Training loss of GPT-2 when training with different rotation dimension n . The loss of performance is consistent across n at our range.

A.2 Reflections and Sampling From The Haar Measure

To sample R_n uniformly from $SO(n)$ with respect to the Haar measure, we employ the QR decomposition trick (Mezzadri, 2007; Ozols, 2009), which samples from the Haar measure μ of the orthogonal group $O(n)$. Let us consider the projection $\pi : O(n) \rightarrow SO(n)$, such that $\pi(\mathbf{R})$ is \mathbf{R} when $\mathbf{R} \in SO(n)$, and $\pi(\mathbf{R})$ simply multiplies the first column of \mathbf{R} by -1 when $\mathbf{R} \in O(n) \setminus SO(n)$. The push forward of μ by π is the Haar measure on $SO(n)$. Since Adam is reflection equivariant, rotating with $\pi(\mathbf{R})$ and with \mathbf{R} will lead to identical performance for any $\mathbf{R} \in O(n)$. Thus we can omit to apply π , and simply sample from μ using the QR decomposition method.

Similarly, Adam is permutation equivariant, thus we omit to apply the inverse permutation before providing the rotated gradients to Adam, and to apply the permutation before rotating the update, as removing these two steps do not affect performances.

A.3 Rotation Residual

Based on the type of rotation and the chosen dimension n , the number of blocks may not divide evenly, i.e., $\frac{d}{n} \notin \mathbb{N}$. To address this issue, we introduce an additional rotation matrix, which we refer to as the *residual* matrix, to complete the missing dimensions. More formally, let d represent the dimensionality of the parameter space, and let n denote the block dimensions of the rotation. We define $b \triangleq \lfloor \frac{d}{n} \rfloor$ as the number of complete blocks. The

residual matrix \mathcal{R} is then sampled from $SO(p)$, where $p \triangleq d - nb$. Therefore, eq. (3) becomes

$$g^{(\mathbf{R}_n, \mathcal{R}, \pi)} := \pi^{-1} \circ ([B \oplus \mathcal{R}] (\pi \circ g)), \quad (5)$$

$$(6)$$

$$= \pi^{-1} \circ \begin{bmatrix} B & \\ & \mathcal{R} \end{bmatrix} (\pi \circ g), \quad (7)$$

$$= \pi^{-1} \circ \begin{bmatrix} R_n & & & & \\ & R_n & & 0 & \\ & & \ddots & & \\ & 0 & & R_n & \\ & & & & \mathcal{R} \end{bmatrix} (\pi \circ g). \quad (8)$$

where $B = \bigoplus_{i=1}^b R_n$.

A.4 Overall Validation and Impact of Flash Attention

In Figure 10, we present the training loss when training GPT-2 with SGD without rotations, with global random rotations using flash attention, and with global random rotations without flash attention. In particular, we confirm two important observations:

- Without flash attention (the setting we use for our experiments) the performances of SGD under global random rotation and under no rotations are identical. This validates that our experimental setting is behaving as expected.
- When we use flash attention with rotations, we observe a slight difference in performance. As explained in Section 2.3, this is due to flash attention amplifying numerical errors from the application of the rotation. Interestingly, likely due to a slight regularization effect, it slows down performance at first but actually provides a small improvement to the loss at the end of training.

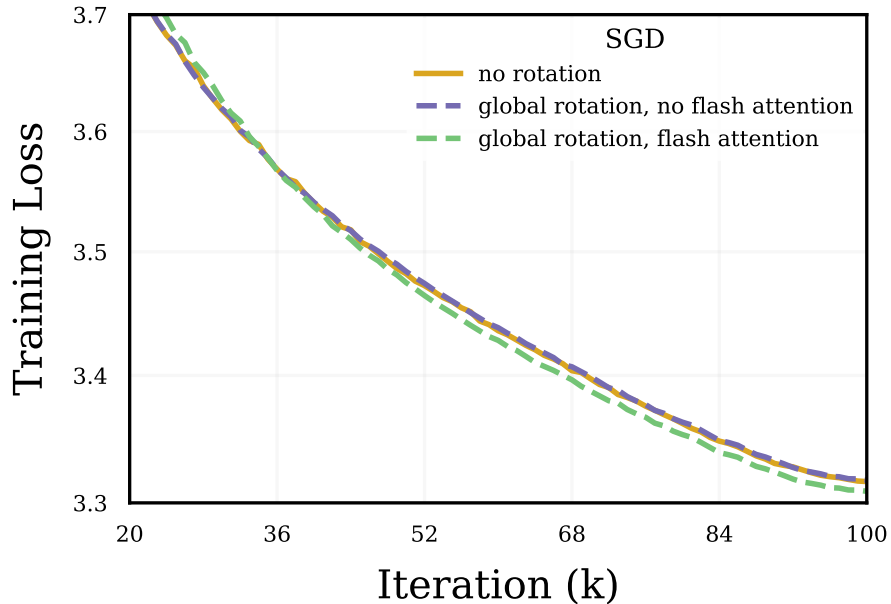


Figure 10: SGD performance when applying global random rotations, with and without flash attention.

B EXPERIMENTAL DETAILS

This section provides additional details about the hyperparameters used for the architecture mentioned in the paper, as well as their optimizer and rotations.

B.1 Rotations Design Choices

By default, for random rotations we fix the dimension of our rotation matrix \mathbf{R}_n at 768 (which is the hidden dimension and thus makes residual rotations unnecessary for most rotation types). The matrix is sampled at the start of training, remains fixed throughout, and is shared across blocks the entire training process.

SVD Rotation. Following Zhao et al. (2024), this is the only rotation that is dynamic rather than static. Specifically, we compute the full-rank SVD decomposition of the gradient for each layer every 250 steps (recommended frequency in Zhao et al. (2024)).

Rotation in Transformers. By default, many implementations store the query, key, and value parameters within a single linear layer. Thus, we split them to treat them as separate layers, reflecting the fundamental differences in how their parameters are involved in forward computations. Additionally, PyTorch stores parameters as tensors in the shape (output_dim, input_dim), but embeddings are stored as lookup tables in the shape (input_dim, output_dim). For output neuron and input neuron rotations to behave intuitively, we thus transpose embedding layers before and after rotations.

B.2 Architectures

GPT2 (Transformer). We trained a GPT-2 model with 124M parameters on the OpenWebText dataset (Gokaslan and Cohen, 2019) using a configuration designed for efficient pretraining. The model architecture includes 12 layers, 12 attention heads, and a 768-dimensional embedding space, with no bias in LayerNorm or Linear layers. We employed the AdamW optimizer with a peak learning rate of $6e-4$, $\beta_1 = 0.9$, $\beta_2 = 0.95$, and a weight decay of $1e-1$, applying gradient clipping of 1.0. Training ran for 100,000 iterations (or 30,000 for some smaller ablations), with learning cosine rate decay starting after a 2,000-iteration warm-up, decaying to a minimum of $6e-5$. We used batch size of 12 with gradient accumulation steps simulating an effective batch size of 40. All experiments were performed on four A100 80GB GPUs, leveraging mixed precision. Unless otherwise specified, all optimizer hyperparameters were shared across experiments and set to the default values specified in Karpathy (2022).

ViT (Vision Transformer). We trained a Vision Transformer (ViT) model on the ImageNet-1K dataset (Deng et al., 2009) using the SimpleViT architecture (Beyer et al., 2022). The model consists of 12 layers, 6 attention heads, a hidden dimension of 384, and an MLP dimension of 1536, with a patch size of 16 and input image size of 224. The AdamW optimizer was employed with a learning rate of 0.001, $\beta_1 = 0.9$, $\beta_2 = 0.999$, $\epsilon = 1e-8$, and a weight decay of 0.1. We used a cosine learning rate schedule with 5 warm-up epochs. The training was conducted for 100 epochs with a batch size of 1024. All experiments were performed with mixed precision.

ResNet-50 (CNN). We trained a ResNet-50 model (He et al., 2015) on the ImageNet-1K dataset (Deng et al., 2009) using the AdamW optimizer. The optimizer was configured with a learning rate of 0.001, $\beta_1 = 0.9$, $\beta_2 = 0.999$, $\epsilon = 1e-8$, and a weight decay of 0.0001. We employed a cosine learning rate schedule with 5 warm-up epochs. The training ran for 100 epochs with a batch size of 256.

B.3 Assumptions Estimation

We now outline how we computed empirical estimations of assumptions in Section 4.

L_∞ -bounded gradient. Algorithm 1 describes the process we use to estimate the bound constant \tilde{C} of stochastic gradients under L_∞ norm, as detailed in section 4.1.

(1,1)-Norm. Using the Hessian rows sampled from GPT-2 checkpoints that were trained under various rotations in Section 4.2, we estimate $\frac{\|H\|_{(1,1)}}{d}$ by averaging the L_1 norm of sampled rows. While this could induce a large

Algorithm 1 Empirical Gradient Bound Estimation for Adam

Require: T : total number of iterations (1000)

Require: $w_{\mathbf{R}'}$: last checkpoint obtained by running Adam under rotation \mathbf{R}'

- 1: Initialize $\tilde{C} \leftarrow 0$ ▷ Maximum infinity norm of gradients
 - 2: **for** $t \leftarrow 1$ **to** T **do**
 - 3: Sample a minibatch B_i ▷ Select one minibatch
 - 4: $g_{B_i} \leftarrow \nabla f_{B_i}^{(\mathbf{R})}(w_{\mathbf{R}'})$ ▷ Compute gradient for minibatch
 - 5: $\tilde{C}' \leftarrow \|g_{B_i}\|_{\infty}$ ▷ Compute infinity norm of the gradient
 - 6: $\tilde{C} \leftarrow \max(\tilde{C}, \tilde{C}')$ ▷ Update the maximum gradient bound
 - 7: **end for**
 - 8: **return** \tilde{C} ▷ Return the estimated gradient bound
-

variance from the sampling of rows, we find that variations of the L_1 norms from rotations are fairly homogeneous across rows.

C ADDITIONAL RESULTS

C.1 Main Experiments

We provide additional results from our main line of experiments.

ViT/S (ImageNet). Figure 11 extends the results from Figure 1b with validation loss and accuracy

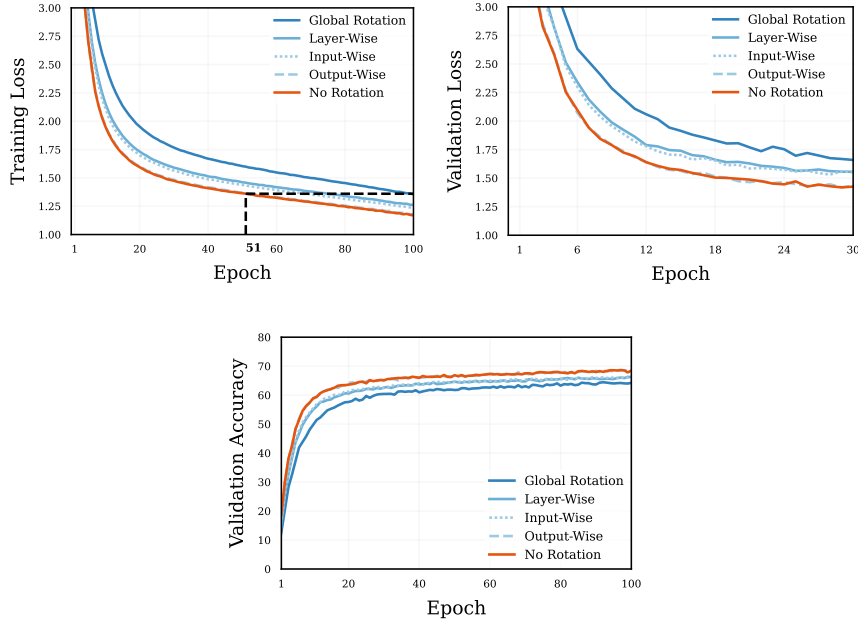


Figure 11: SimpleViT - Imagenet training loss, validation loss and top-1 validation accuracy

ResNet50 (ImageNet). Figure 12 demonstrates that Adam maintains its performance well under rotational transformations for ResNets. This robustness to rotation implies that Adam gains little advantage from the standard basis structure in this setting. This finding aligns with the fact that SGD with extensive tuning can outperform Adam when training these networks.

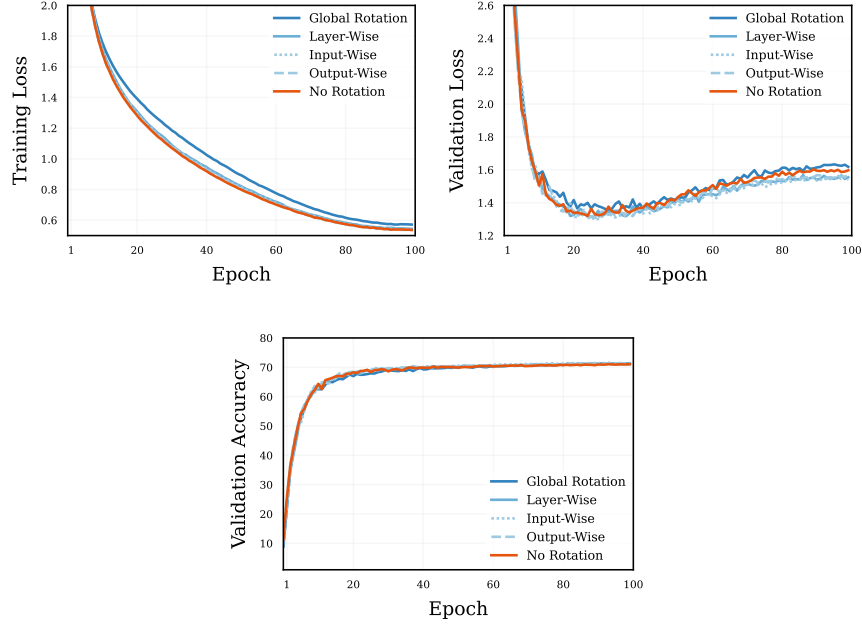


Figure 12: Training loss, validation loss and top 1 % validation accuracy, when training a ResNet-50 with Adam on ImageNet across different scopes of rotations.

C.2 Architecture Aware Rotation.

We seek to identify whether certain transformer layer types are more sensitive to rotations than other, and contribute more to the overall performance degradation observed in Figure 1a when using layer-wise rotations.

Figure 13 shows the loss curves when rotating only one layer type at a time. We find that the performance degradation induced by layer-wise rotations is small for most layer types, seemingly balanced across these layers, with the exception of value and embedding layers.

Layerwise rotation of value layers seem to impact the loss more noticeably than with other layer types. In Figure 15, we find that reducing the scope of rotations to output neuron wise does not improve the performance when rotating value layers.

The biggest drop of performances is observed for embedding layers, which we conjecture to be linked to the discrepancy in frequency across tokens. Figure 14 shows indeed that when rotating the embedding layer by output neuron (i.e., within weights corresponding to a same token) the degradation becomes unnoticeable.

C.3 Hessian Rows

We use the end checkpoint of GPT2 to sample rows from the Hessian in different rotated parameter spaces (see Section 4.2).

From Figure 16 to Figure 22, we present the same figure as in Figure 7, but for rows taken from different layer types, confirming that the behavior we observed is consistent across parameter types. Except for embeddings, rows are always taken from the second Transformer block.

Figure 23 shows a row in the attention projection layer of the 8-th transformer block, showing our observations seem also consistent across depth.

Figure 24 uses checkpoints trained with the same rotations as the one applied to the Hessian. We find the same behavior for no rotations, global and output-wise, but we find that with the SVD-rotated checkpoints, there is increased variance in the Hessian values outside of the layer.

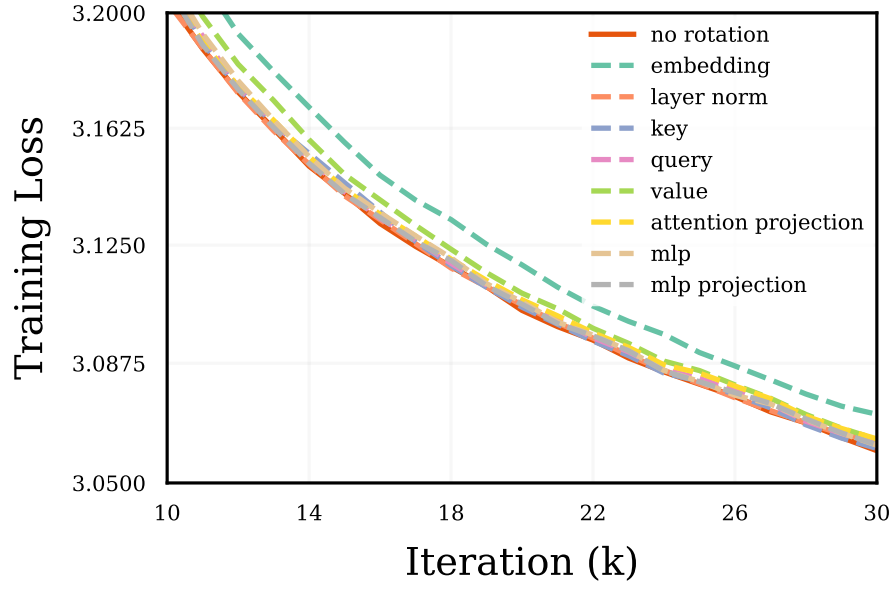


Figure 13: Layer-wise rotation applied to only specific layer types

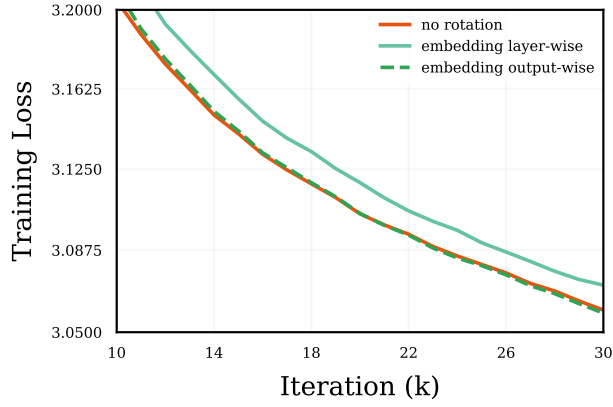


Figure 14: Layer-wise rotation and output-wise rotation on embedding layers only

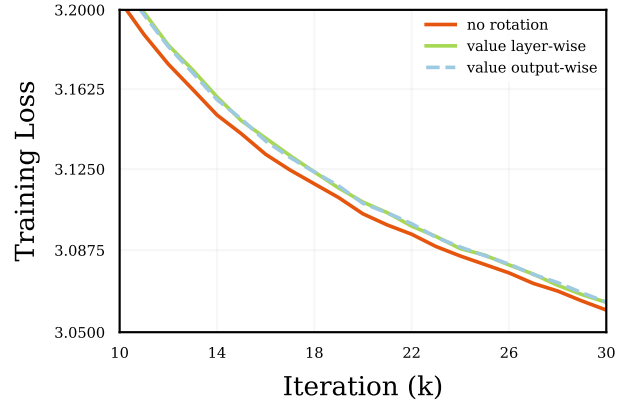


Figure 15: Layer-wise rotation and output-wise rotation on attention values only

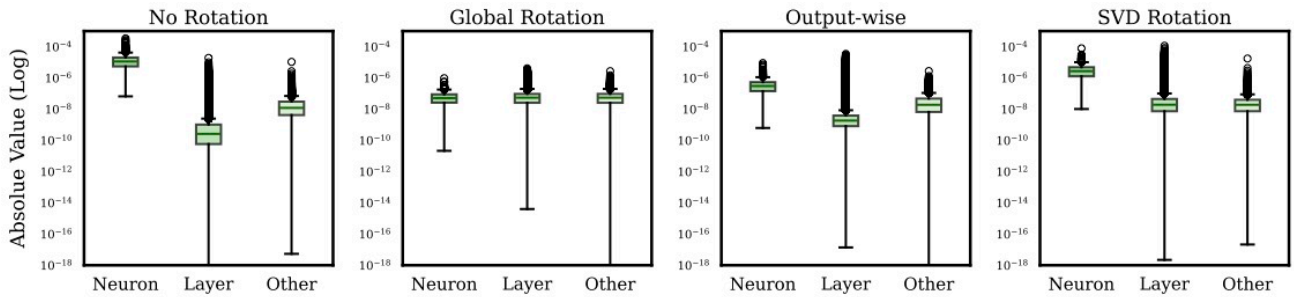


Figure 16: Hessian value distribution of a row in embedding layer.

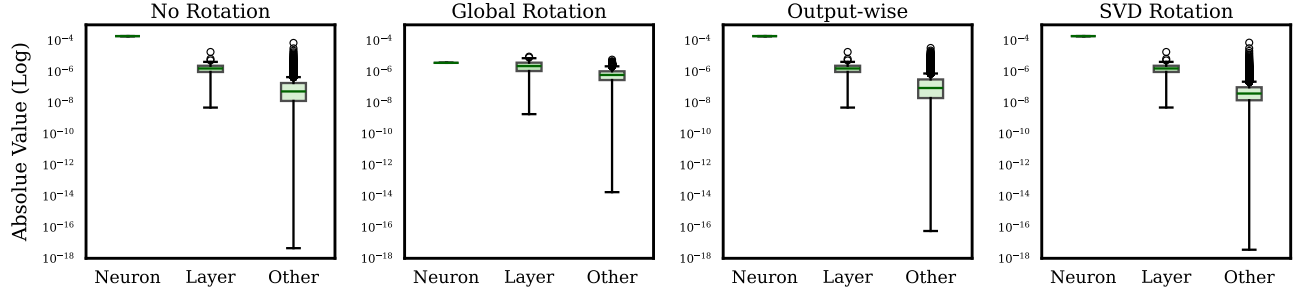


Figure 17: Hessian value distribution of a row in second Transformer layer norm layer.

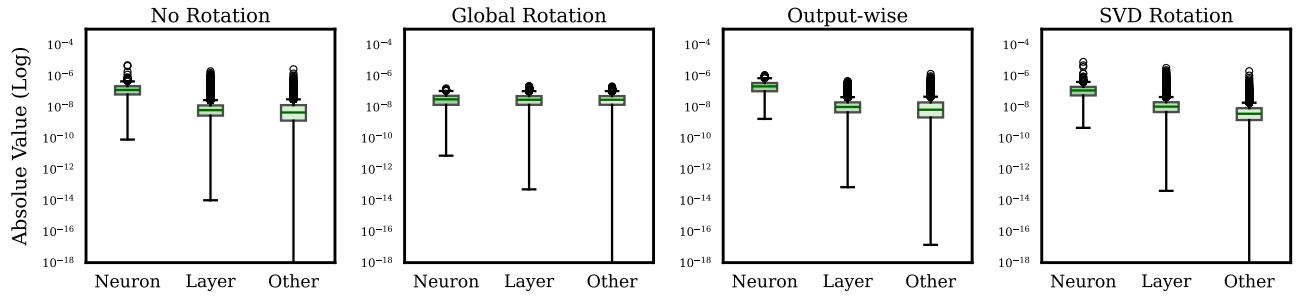


Figure 18: Hessian value distribution of a row in second Transformer key layer.

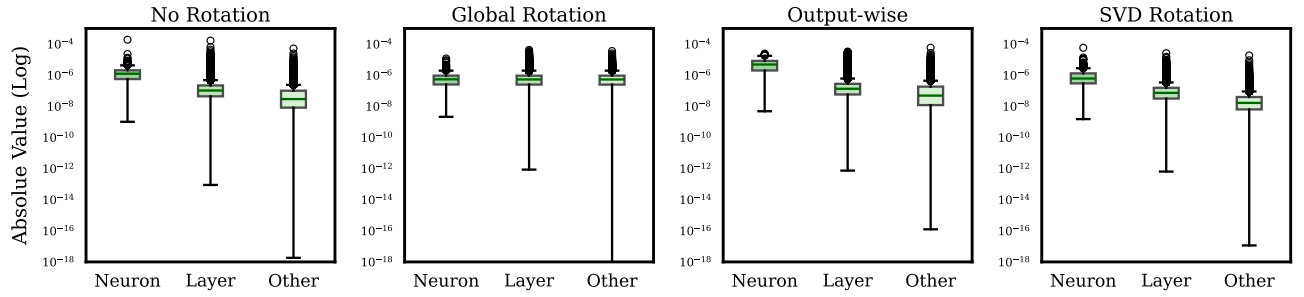


Figure 19: Hessian value distribution of a row in second Transformer query layer.

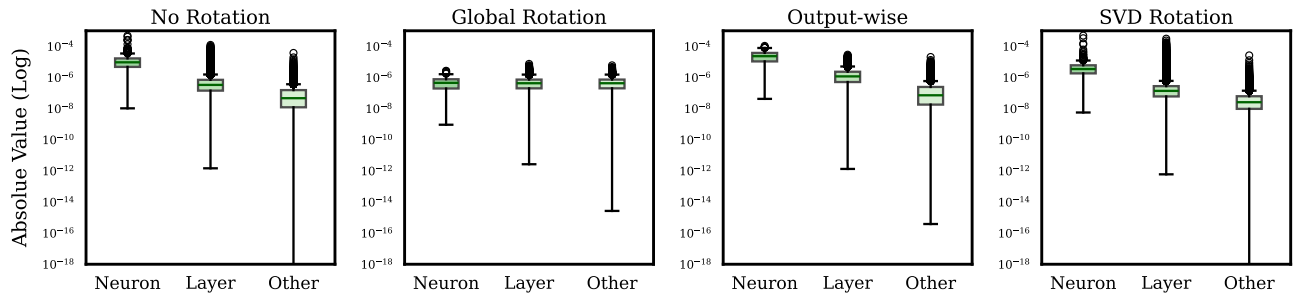


Figure 20: Hessian value distribution of a row in second Transformer value layer.

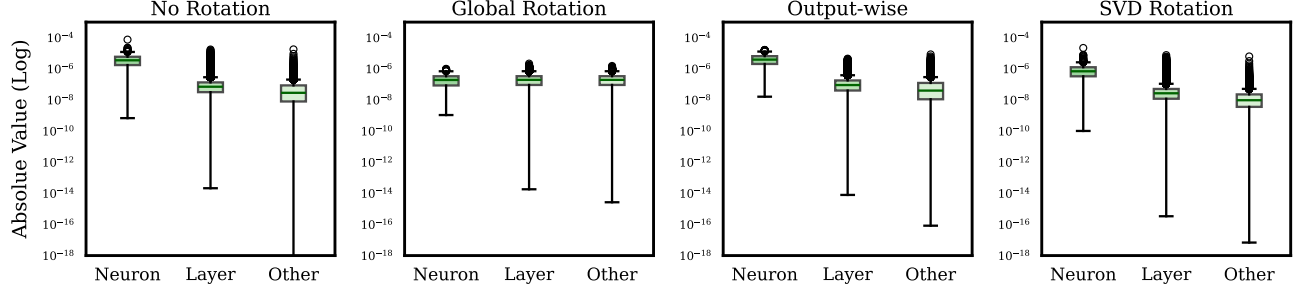


Figure 21: Hessian value distribution of a row in second Transformer mlp layer.

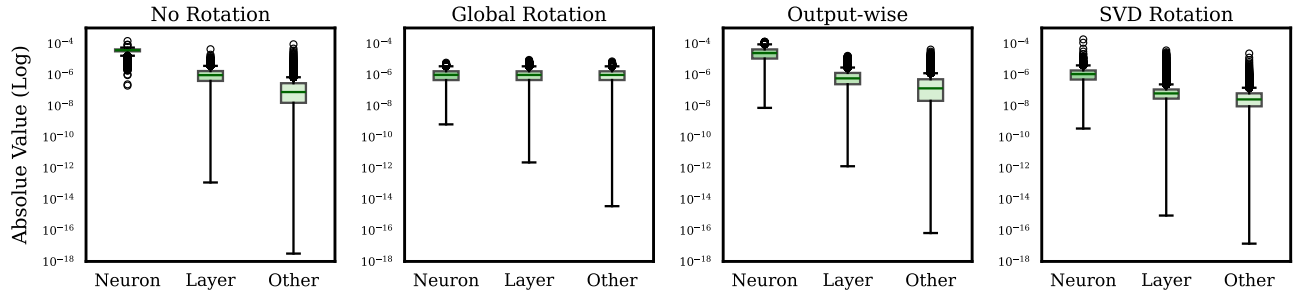


Figure 22: Hessian value distribution of a row in second Transformer mlp projection layer.

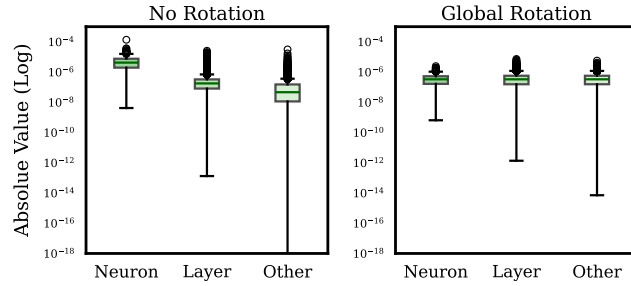


Figure 23: Hessian value distribution of a row in eighth Transformer attention projection layer.

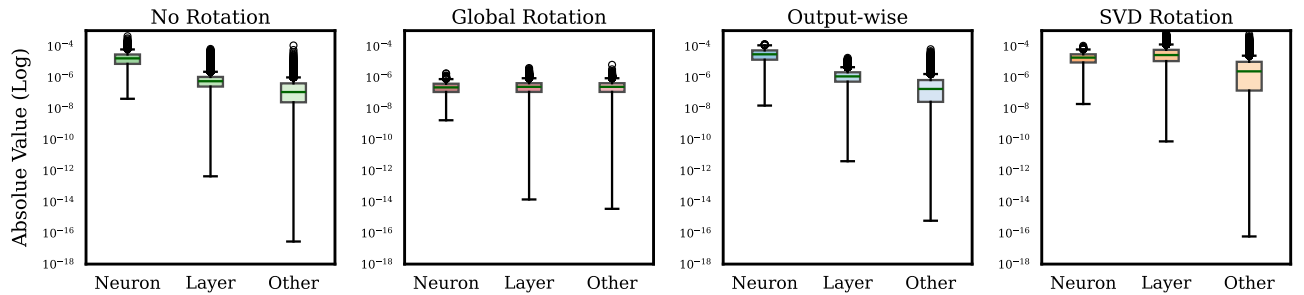


Figure 24: Hessian value distribution of a row in second Transformer attention projection layer from checkpoints that are *trained with different rotations*.

D ADAMW ALGORITHM

We remind here the AdamW algorithm (pseudocode) in Algorithm 2, and provide a rotated version in Algorithm 3.

Algorithm 2 AdamW Optimization Algorithm

Require: α : stepsize
Require: $\beta_1, \beta_2 \in [0, 1)$: exponential decay rates for moment estimates
Require: λ : weight decay coefficient
Require: ϵ : small constant for numerical stability
Require: $f(\theta)$: stochastic objective function with parameters θ

- 1: Initialize $\theta_0, m_0 \leftarrow 0, v_0 \leftarrow 0, t \leftarrow 0$
- 2: **while** θ_t not converged **do**
- 3: $t \leftarrow t + 1$
- 4: $g_t \leftarrow \nabla_{\theta} f_t(\theta_{t-1})$ ▷ Get gradients w.r.t. stochastic objective at timestep t
- 5: $m_t \leftarrow \beta_1 \cdot m_{t-1} + (1 - \beta_1) \cdot g_t$ ▷ Update biased first moment estimate
- 6: $v_t \leftarrow \beta_2 \cdot v_{t-1} + (1 - \beta_2) \cdot g_t^2$ ▷ Update biased second raw moment estimate
- 7: $\hat{m}_t \leftarrow m_t / (1 - \beta_1^t)$ ▷ Compute bias-corrected first moment estimate
- 8: $\hat{v}_t \leftarrow v_t / (1 - \beta_2^t)$ ▷ Compute bias-corrected second raw moment estimate
- 9: $\theta_t \leftarrow \theta_{t-1} - \alpha \cdot \hat{m}_t / (\sqrt{\hat{v}_t} + \epsilon) - \alpha \cdot \lambda \cdot \theta_{t-1}$ ▷ Update parameters
- 10: **end while**
- 11: **return** θ_t ▷ Return the final parameters

Algorithm 3 AdamW Optimization Algorithm with Rotation

Require: α : stepsize
Require: $\beta_1, \beta_2 \in [0, 1)$: exponential decay rates for moment estimates
Require: λ : weight decay coefficient
Require: ϵ : small constant for numerical stability
Require: $f(\theta)$: stochastic objective function with parameters θ

- 1: Initialize $\theta_0, m_0 \leftarrow 0, v_0 \leftarrow 0, t \leftarrow 0$
- 2: **while** θ_t not converged **do**
- 3: $t \leftarrow t + 1$
- 4: $g_t \leftarrow \nabla_{\theta} f_t(\theta_{t-1})$ ▷ Get gradients w.r.t. stochastic objective at timestep t
- 5: $\tilde{g}_t = R \cdot g_t$ ▷ Apply rotation to gradients
- 6: $m_t \leftarrow \beta_1 \cdot m_{t-1} + (1 - \beta_1) \cdot \tilde{g}_t$ ▷ Update biased first moment estimate
- 7: $v_t \leftarrow \beta_2 \cdot v_{t-1} + (1 - \beta_2) \cdot \tilde{g}_t^2$ ▷ Update biased second raw moment estimate
- 8: $\hat{m}_t \leftarrow m_t / (1 - \beta_1^t)$ ▷ Compute bias-corrected first moment estimate
- 9: $\hat{v}_t \leftarrow v_t / (1 - \beta_2^t)$ ▷ Compute bias-corrected second raw moment estimate
- 10: $\theta_t \leftarrow \theta_{t-1} - \alpha \cdot R^{-1} \cdot (\hat{m}_t / (\sqrt{\hat{v}_t} + \epsilon)) - \alpha \cdot \lambda \cdot \theta_{t-1}$ ▷ Update parameters
- 11: **end while**
- 12: **return** θ_t ▷ Return the final parameters

E COMMON ASSUMPTIONS IN FIRST-ORDER OPTIMIZATION THEORY

We present a non-exhaustive summary of common assumptions used in theoretical works for first-order optimization, see Table 3. For each assumption, we indicate whether it is rotation invariant.

Assumption	Rotation-Invariant
(Strong-) Convexity	✓
Polyak-Lojasiewicz (Polyak, 1963)	✓
Star-(Strong)-Convexity (Guille-Escuret et al., 2020)	✓
Quadratic Growth (Goujaud et al., 2022)	✓
L-Smoothness (L_2 norm) (Défossez et al., 2022; Zhou et al., 2024)	✓
Gradient Growth Condition (Zhang et al., 2022)	✓
Bounded Expected Gradient Squared Norm (Zou et al., 2019)	✓
(L_0, L_1) -Smoothness (Li et al., 2023b)	✓
Restricted Secant Inequality (Guille-Escuret et al., 2022)	✓
Error Bound (Luo and Tseng, 1993; Guille-Escuret et al., 2024)	✓
L-smoothness (L_∞ norm)(Guo et al., 2022)	✗
Coordinate-wise (L_0, L_1) -Smoothness (Crawshaw et al., 2022)	✗
Coordinate-wise “Affine” Variance Noise (Li and Lin, 2024)	✗
Bounded Gradient (L_∞) (Reddi et al., 2018)	✗

Table 3: Common assumptions involved in first-order optimization algorithm, indicating whether they are rotation-invariant. Rotation-dependent assumptions are comparatively rare in the literature.